This is the Pre-Published Version.

This version of the article has been accepted for publication, after peer review (when applicable) and is subject to Springer Nature's AM terms of use(https://www.springernature.com/gp/open-research/policies/accepted-manuscript-terms), but is not the Version of Record and does not reflect post-acceptance improvements, or any corrections. The Version of Record is available online at: http://dx.doi.org/10.1007/s11661-021-06204-w.

Atomistic Simulation on the Mechanical Properties of Diffusion Bonded Zr-Cu Metallic Glasses with Oxidized Interfaces

Tian Li [a], Guangping Zheng [a,*]

[a] *Department of Mechanical Engineering, Hong Kong Polytechnic University, Hung Hom, Kowloon, Hong Kong SAR, 10000, China*

* To whom correspondence should be addressed. E-mail: mmzheng@polyu.edu.hk

ABSTRACT

A novel welding technique of diffusion bonding for Zr-Cu metallic glass with pre-oxidized surfaces is proposed in this study, which is systematically investigated by molecular dynamics (MD) simulation. Compared with the conventional welding technique, the diffusion bonding process can be well implemented below the crystallization temperature of metallic glass. The obtained structure possesses glass-glass interfaces (GGIs) similar with those in nano-glasses. As revealed by MD simulation, the diffusion bonded metallic glasses possess enhanced mechanical strength and ductility that generally do not exist in nano-glasses and their bulk metallic glass counterparts. The GGIs are found to hinder the propagation of shear bands, where there is strong bonding between Zr and O and the segregated Cu and ZrO_2 clusters could induce extra plasticity. The results demonstrate that the diffusion bonding of metallic glass with pre-oxidized surfaces could provide an alternative approach in solving the longstanding issue of size limitation on metallic glasses.

I. INTRODUCTION

Amorphous alloys, also known as metallic glasses (MGs), possess outstanding mechanical properties including high mechanical strength and excellent corrosion resistance, and are promising for structural applications [1]-[2]. Even though different MGs with a variety of compositions have been fabricated in the past decades, the MGs are still not large enough in physical dimensions (< 10 cm) due to the fast quenching rate required for suppressing crystallization. Meanwhile, conventional welding technique cannot be applied to MGs due to high temperature profiles at heat affected zone (HAZ) that might induce crystallization. The mechanical properties of MG might be greatly deteriorated if low-temperature (< 500 ^{o}C) solders are used in the welding process. Therefore, to overcome the size limitation on MGs, other welding techniques for MGs should be further investigated and developed. By far, only a few studies have been reported, demonstrating the feasibility of friction, electron-beam, spark, pulse-current and explosive jointing techniques in wedding MGs [3]–[7]. However, those alternative approaches are not suitable for massive manufacturing and the processing parameters must be precisely controlled. Moreover, the mechanical performances of MGs welded by those approaches are at best compatible to those of as-prepared MGs.

Recently, a novel type of nanomaterial, named as nano-glass, has been successfully prepared, which consists of numerous glass-glass interfaces (GGI) connecting different nano-sized MG clusters or particles [8]–[11]. It is mainly synthesized by inert gas condensation, magnetron sputtering, serve plastic deformations and electrodeposition. Among these techniques, inert gas condensation is the most commonly used one, which produces nano-glasses by compacting nano-sized MG clusters under high external pressure (>100 MPa) and

at ambient or elevated temperatures [12]-[13]. Such formation of nano-glasses can be considered as diffusion bonding, and could be promising in solving the longstanding issue of size limitation on MGs. Moreover, the ductility of as-prepared nano-glasses is found to be enhanced, compared to those of their bulk MG counterparts [14]–[25]. On the other hand, the viability of diffusion bonding for nano-glass fabrication under ambient conditions, e.g., without the protection of inert gases, becomes critical and the formation of GGIs among different MG clusters must be facile to eliminate the manufacturing barrier, for example, through the powder metallurgy manufacturing route. Nonetheless, one of the challenging issues of handling nano-sized MG clusters or powders in those manufacturing routes is the oxidation inevitably occurred on the surfaces of MGs. Thus, it is necessary to understand the effects of oxidized layers of the nano-sized MG clusters on the diffusion bonding of nano-glasses.

In this study, we investigate the diffusion bonding of MG blocks with oxidized surfaces since surface oxidation of nano-sized MG blocks cannot be avoided at ambient processing conditions. From molecular dynamics (MD) simulation, the pre-oxidized surfaces are found to facilitate the formation of GGIs at different diffusion bonding temperatures under atmospheric pressure, firmly connecting the nano-sized MG blocks and resulting in multilayer structures. Furthermore, the mechanical properties of the diffusion bonded MGs are predicted and the size effects of oxidized MG blocks on their mechanical properties are investigated.

II. SIMULATION METHODOLOGIES

The MD simulations were performed using Large-Scale Atomic/Molecular Massively Parallel Simulator (LAMMPS) [26]. A representative crystalline $Zr_{50}Cu_{50}$ alloy with dimensions of $5 \times 5 \times 5$ nm^3, roughly 7000 atoms, was constructed using ATOMSK software [27] and initially relaxed at 300 K for 100 ps under zero external pressure. Periodic boundary conditions (PBCs) were applied and the embedded atom method (EAM) [28] was used to describe the inter-atomic interactions of Zr-Zr, Zr-Cu and Cu-Cu atoms. Then the system was heated gradually and equilibrated at 2000 K (above the melting temperature T_m = 1400 K) for 2 ns to allow for the complete melting of $Zr_{50}Cu_{50}$, and the melt was quenched to 300 K at a cooling rate of 10^{12} K s^{-1} and relaxed for 500 ps. The obtained $Zr_{50}Cu_{50}$ was further analyzed by radial distribution function that confirmed its amorphous structure. Subsequently, a replicated MG block was placed at the other side and an additional O_2 layer was inserted between two MG blocks. As shown in Fig. 1(a), the surface of each MG block was exposed to O_2. Oxidation at the exposed MG surfaces under zero external pressure was simulated at 300-600 K for 2 ns by using canonical-ensemble (NVT) MD. The Charge-Optimized Many-Body (COMB3) potential [29] was used to describe the inter-atomic interactions of Zr-O, Cu-O and O-O atoms. After the oxidation, the extra O_2 molecules were removed and the remained MG blocks with oxidized surfaces were consolidated for 2 ns under a hydrostatic pressure of 1 bar at 400, 500, 600 and 700 K (the glass transition temperature T_g = 670 K), separately. After the bonding process, the system was equilibrated at 300 K for 1 ns, resulting in the diffusion bonded MG structure with one GGI, as shown in Fig. 1 (b). In order to investigate the size effects on the mechanical properties of the diffusion bonded MGs, MG blocks with oxidized surfaces (Fig. 1c) which had roughly 10000, 20000, 30000, 40000 and 60000 atoms and were 2.5, 5, 10, 15, 20 nm in thickness, were consolidated at 600 K under a hydrostatic pressure of 1 bar, as simulated by isobaric-isothermal (NPT) ensemble MD. Different from the previously obtained

systems with one GGI only, the systems containing MG blocks with different thicknesses contained two GGIs, as shown in Fig. 1 (d). In the aforementioned MD simulations of oxidation and diffusion bonding processes, PBC was applied in each direction and the finally obtained diffusion bonded MGs formed the multilayer structures, as shown in Fig. 1.

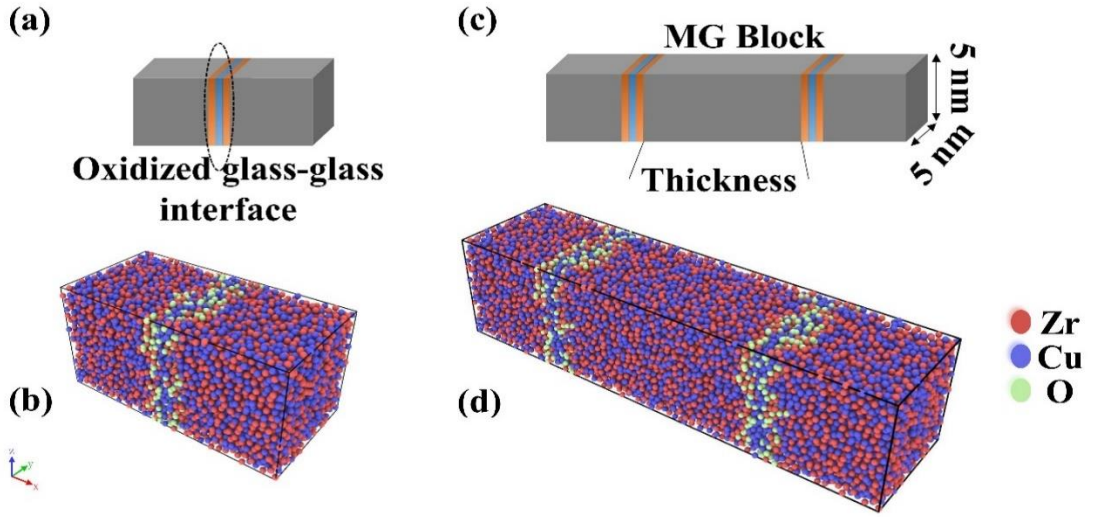

Fig. 1. Schematics of diffusion bonded $Zr_{50}Cu_{50}$ MGs with (a) one GGI, and (c) two GGIs, whose atomic structures are shown in (b) and (d), respectively.

All diffusion bonded systems were equilibrated at 300 K for 2 ns before the uniaxial tensile loading was applied in *x*-direction at a strain rate of 3.33 x 10^7 s^{-1}. There were lateral tractions at *y*- and *z*-directions during the tensile loading process, and the temperature was kept at 300 K by using a Nose-Hoover thermostat in NVT ensemble MD simulation. The atomistic mechanisms of diffusion bonding and mechanical deformation were analyzed by self-scripted MATLAB code and visualized by OVITO software packages [30].

III. RESULTS AND DISCUSSION

The diffusion bonded MGs with one and two GGIs are shown in Fig. 1 (b) and (d), respectively, clearly indicating that the GGIs have different atomic structure with the MG blocks. The mechanical properties of diffusion bonded Zr-Cu MGs with one oxidized GGI, which contain 10 nm Zr-Cu MG blocks welded at different temperatures, are investigated by the tensile tests. The engineering stress vs. strain curves, presented in Fig. 2 (a), reveal that the Zr-Cu MGs are well bonded together, without showing a sudden stress drop with a strain lower than the elastic limit of Zr-Cu MGs (~2%). After reaching its ultimate tensile strength (UTS) at 1.52 -1.75 GPa, the engineering stress starts decreasing until the fracture occurs. It is found that the welded Zr-Cu MGs with oxidized GGI could have enhanced UTS and ductility as measured by the plastic strain at the UTS, in comparison with those of pristine MGs (Fig. 2a). Among the systems investigated, Zr-Cu MG bonded at 500 K exhibits the best combination of mechanical strength and ductility, i.e., an extra plasticity of 6.2% and a UTS of 1.75 GPa.

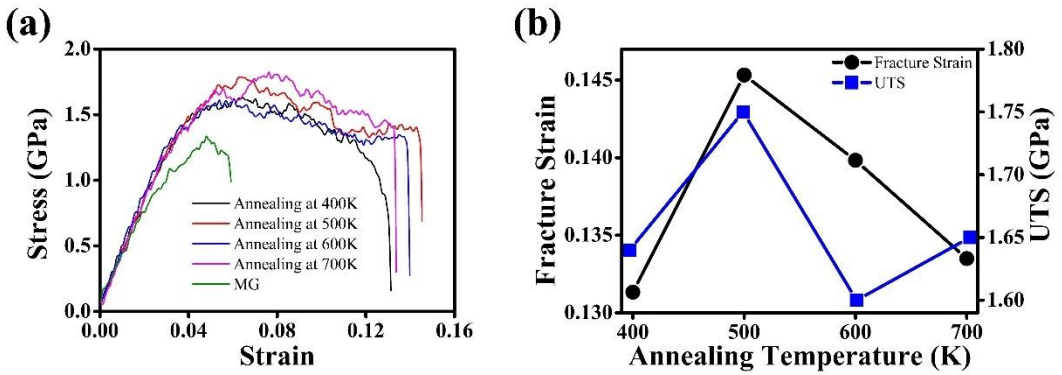

Fig. 2. The mechanical properties of diffusion bonded MGs with MG blocks 10 nm in thickness. (a) Stress vs strain curves for the MGs bonded at different temperatures. (b) The influences of welding temperature on fracture strain and UTS.

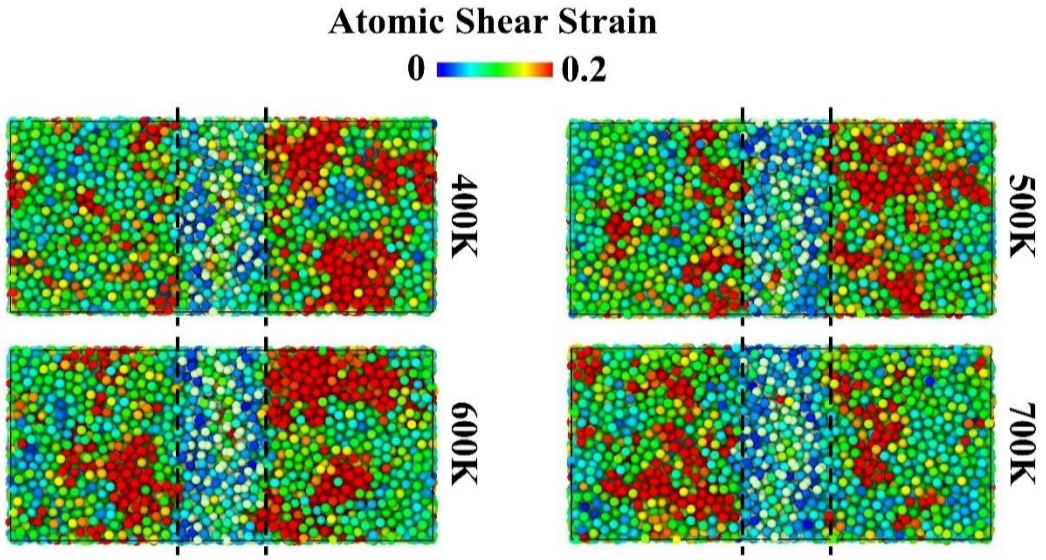

Fig. 3. The atomic shear strain mapping for MGs bonded at 400, 500, 600 and 700 K with an engineering strain of 7.5 %. The dash lines mark the GGI regions.

To have a better understanding on the welding temperature dependence mechanical properties, the mapping of atomic shear strain for each diffusion bonded MG at an engineering strain of 7.5% is shown in Fig. 3, and the shear bands can be identified as those localized regions with high shear strains. Here, the atomic shear strain is defined as [31-34]:

$$\eta_i = \frac{1}{2}(J_i J_i^T - I) \quad , \tag{1}$$

$$\eta_i^{Mises} = \sqrt{\eta_{xy}^2 + \eta_{xz}^2 + \eta_{yz}^2 + \frac{(\eta_{xx}-\eta_{yy})^2+(\eta_{xx}-\eta_{zz})^2+(\eta_{yy}-\eta_{zz})^2}{6}} \quad , \tag{2}$$

where η_i is the local Lagrangian strain matrix for each atom i, J_i is the local transformation matrix and η_i^{Mises} is the atomic shear strain. It can be observed that in the MGs bonded at 500 K, the GGI actively involves in the plastic deformation and the roles of GGI are two folded. The shear bands can be generated from GGI and propagate into the MG blocks, or they are generated inside the MG block and are hindered by the GGI, resulting in the enhanced plasticity

and mechanical strength, respectively. The mapping of shear strain in the MG blocks at both sides of GGI, as shown in Fig. 3, indicates that in the MGs bonded at 500 K there are 5 localized shear regions that can be connected with GGI. For other diffusion bonded MGs at different temperatures (400, 600 and 700 K), on the contrary, the GGI is less involved during the plastic deformation and the number of those regions are only 2 to 3. It could be the reason that their mechanical properties are not compatible to those of MGs bonded at 500 K.

To investigate the size effects on the mechanical properties of diffusion bonded Zr-Cu MGs, MG blocks with different sizes in thickness are oxidized and welded at 600 K. The stress vs. strain curves for diffusion bonded MGs are analyzed, as shown in Fig. 4 (a). The Young's modulus and tensile strength of diffusion bonded MGs are enhanced as the thickness of MG block decreases, while the elongation to failure of diffusion bonded MGs is deteriorated. When the thickness of MG block is lower than 5 nm, its tensile strength is dramatically increased up to 3.7 GPa, as shown in Fig. 4 (b). The tensile strength of diffusion bonded MGs is close to that of pristine MGs when the thickness of MG block is increased to 20 nm. Moreover, the ductility is dramatically improved from 4.8% to nearly 10% when the thickness of MG blocks is reduced to 2.5 nm.

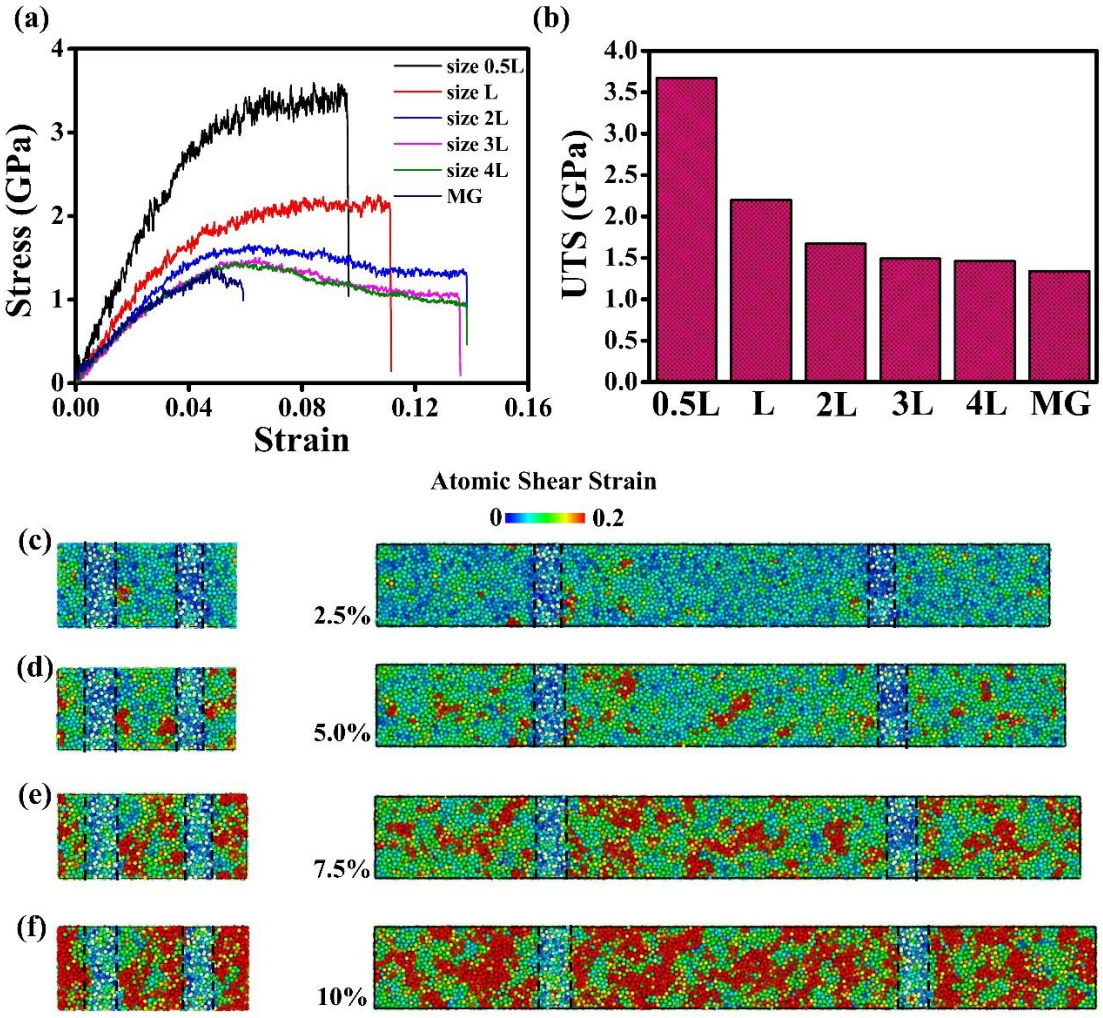

Fig. 4. (a) Stress vs strain curves of the diffusion bonded MGs with MG blocks in different sizes (thicknesses); L=5 nm. (b) The size effects on UTS. Atomic shear strain mapping of diffusion bonded MGs with MG blocks 5-nm (left column) and 20-nm in thickness (right column), which are deformed at

strains of 2.5% (c), 5% (d), 7.5% (e), 10% (f). The dash lines mark the GGI regions.

The mapping of atomic shear strain for the diffusion bonded MGs with 5 and 20 nm MG blocks in thickness is shown in Fig. 4. When the diffusion bonded MGs are under plastic deformation (strain>2%), both systems are deformed heterogeneously with the initiation of shear bands either inside the MG blocks or from the GGIs. At an engineering strain of 5%, the shear bands are found to propagate along the direction with an incline angle of about 45° with the loading direction. In the diffusion bonded MGs with 20 nm MG blocks, most shear bands do not interact with GGIs, and grow across the system in the lateral direction, directly leading to the catastrophic failure of the bonded MGs. However, in the diffusion bonded MGs with 5 nm MG blocks, the shear bands are hindered by GGIs, and as a result, the mechanical strength is enhanced. Fig. 4 (c)-(f) thus demonstrates that the roles of GGI may be different in the diffusion bonded MGs containing MG blocks with different sizes. Therefore, as shown in Fig. 4 (b), the mechanical strength of diffusion bonded MGs is found to significantly increase when the ratio of thickness to lateral dimension of the MG blocks is less than 1.0.

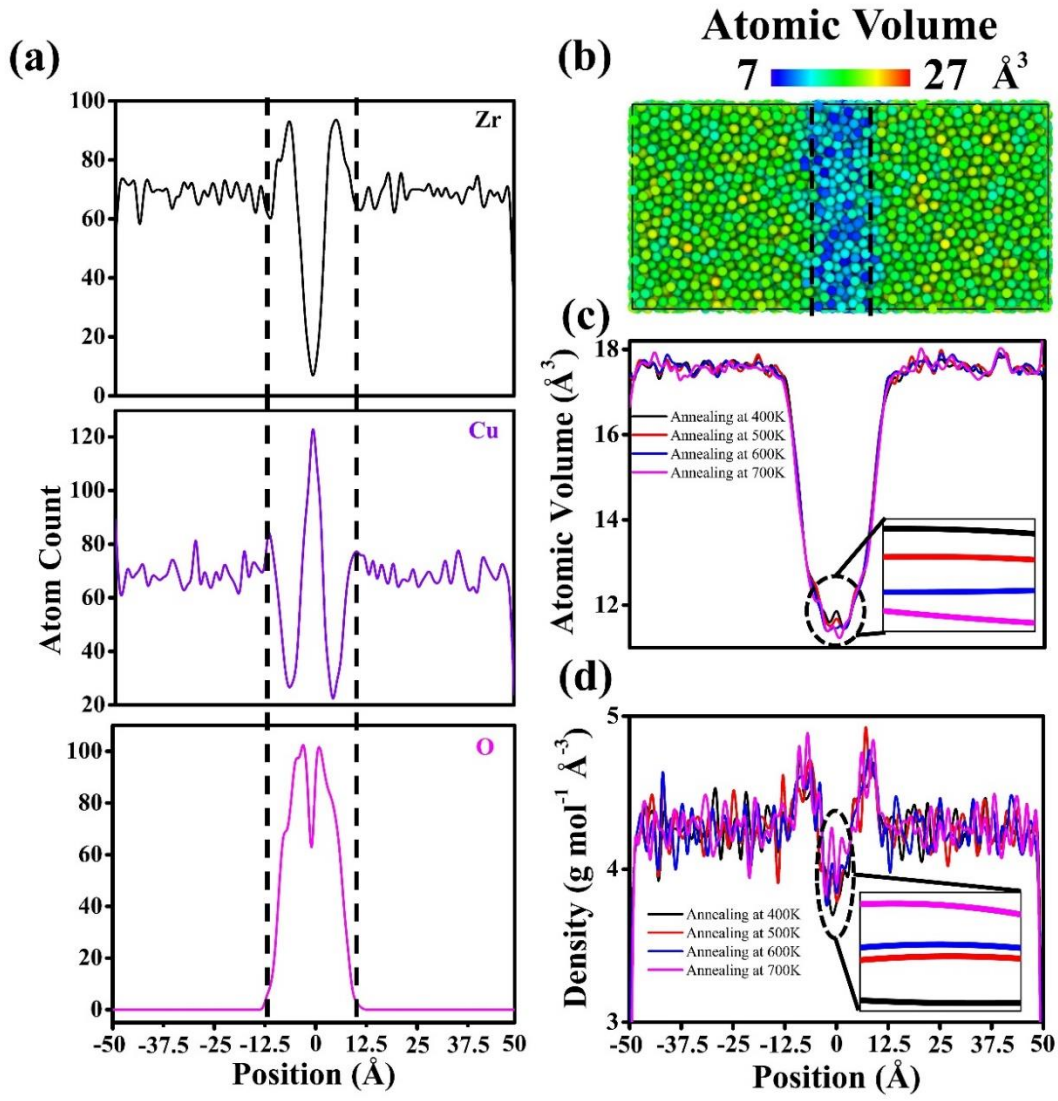

Fig. 5. The chemical composition analysis on oxidized interfaces in the bonded Zr-Cu MGs with L=5 nm: (a) atomic count variation vs position, (b) visualization of atomic volume, (c) atomic volume at the

interface bonded at different welding temperatures, and (d) density at the interface bonded at different temperatures. The dash lines mark the GGI regions.

Since the oxidized interface plays an important role in low-temperature welding and in enhancing mechanical properties of the diffusion bonded MGs, it is necessary to conduct a comprehensive investigation about the structure and composition of oxidized interface for a better understanding about the mechanisms of welding and the enhanced mechanical properties of bonded MGs. In Fig. 5 (a), the composition variation is plotted with respect to the position in the system. It can be seen from the plots that the atoms are evenly distributed in the MG blocks and the composition variation can be observed at the positions close to the oxidized interface. In general, the oxidized interface could be divided into two different regions that consist of different chemical compositions. The Cu atoms are highly concentrated in the center of oxidized interface, where Zr and O atoms are more preferentially located on the MG blocks at both sides of the interface. Compared with the MG blocks, the oxidized interface exhibits a reduced atomic volume, as shown in Fig. 5 (b). However, as the welding temperature is increased, the atomic volume at oxidized interface is further decreased while the density at the interface is enhanced, as shown in the Fig. 5 (c) and (d). Moreover, the density in the center of oxidized interface is determined to be the minimum, less than that of MG blocks. In contrast, the density at both sides of the oxidized interface exhibits the maximum, where Zr and O atoms are enriched. By analyzing the atomic structure, quite a few ZrO_2 clusters, as shown in Fig. 6 (a), have been found at the oxidized interface. Moreover, as shown in Fig. 6(b), a small amount of CuO clusters can be observed at the oxidized interface where Cu atoms seem to be less favorable to interact with O atoms as compared with Zr atoms. The formation of ZrO_2 clusters is critical to the enhanced mechanical properties of the diffusion bonded MGs since the mechanical strength of ZrO_2 crystal is as high as 2000 MPa [35]. On the one hand, the ultimate tensile strength of diffusion bonded MGs could be much enhanced since the ZrO_2 clusters could be hard obstacles that impede the propagation of shear bands generated in the interiors of MG blocks. On the other hand, the formation of ZrO_2 clusters leads to the structural heterogeneity around the GGI, where shear bands could be generated close to the resultant ZrO_2 clusters. Because of the sparse distribution of ZrO_2 clusters, multiplication of shear bands at the ZrO_2 clusters could lead to the enhanced ductility of the diffusion bonded MGs.

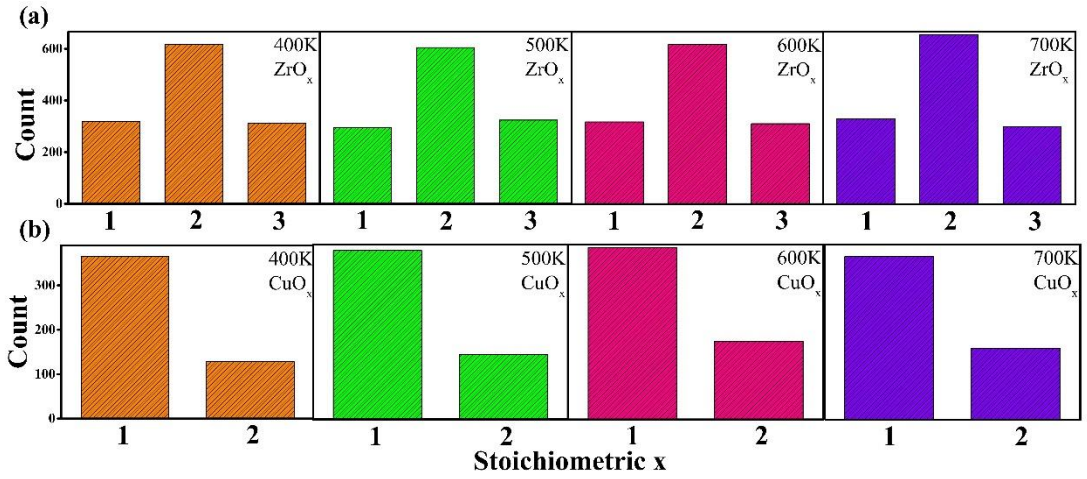

Fig. 6. Analyses on the chemical composition of (a) Zr-O, and (b) Cu-O clusters formed at glass-glass

interfaces in the MGs bonded at different temperatures.

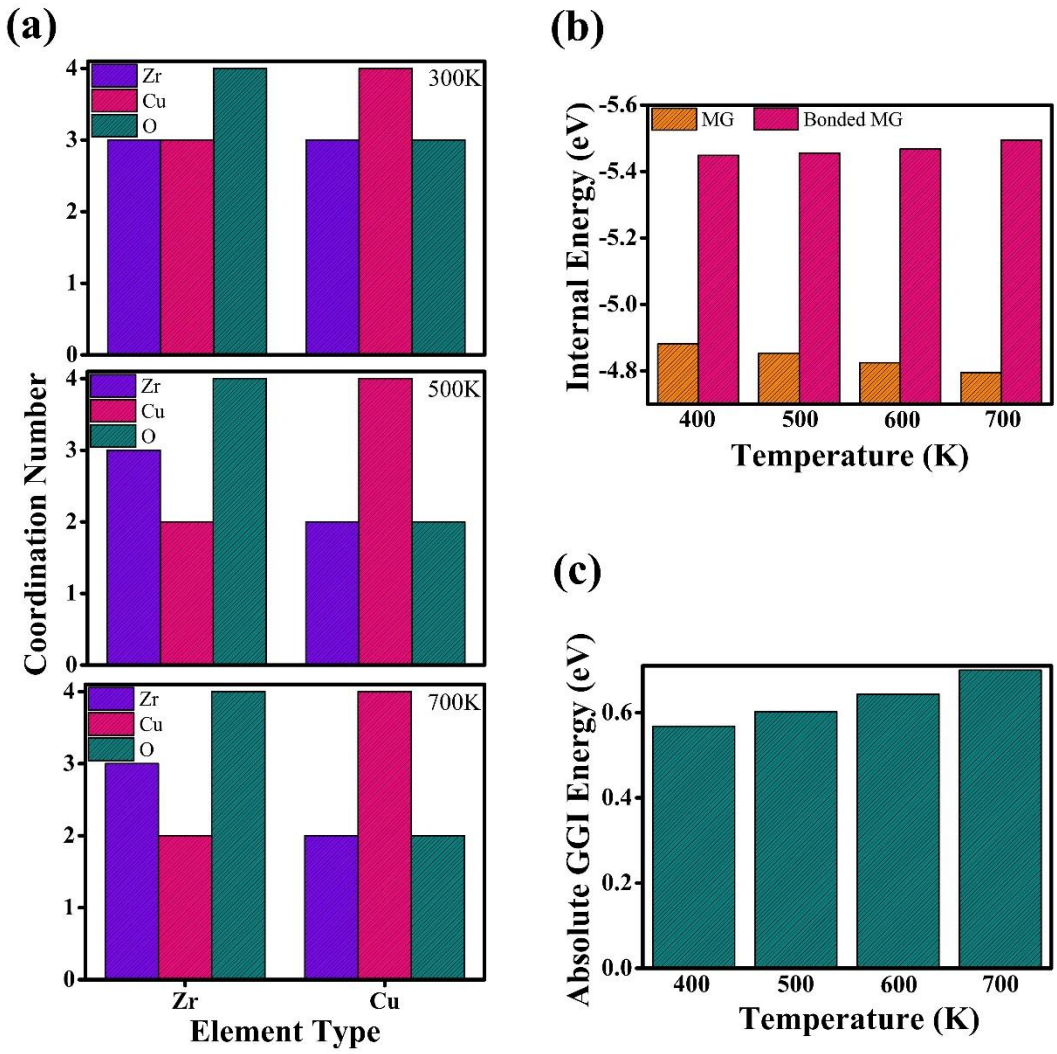

Fig. 7. (a) The coordination analysis on Zr-, and Cu-centered clusters in the MGs bonded at different temperatures. (b) Internal energy of MG and diffusion bonded MGs. (c) Absolute energy of the glass-glass interface.

The atomic coordination of Zr and Cu atoms at the MG surface oxidized under different temperatures are analyzed, as shown in Fig. 7 (a). For all oxidization temperatures, the O atoms, with an approximated average amount of 4 for Zr-centered atom and 2-3 for Cu-centered atom, are more preferential to interact with the Zr atoms. Meanwhile, Cu-centered atom tends to closely interact with other Cu atoms, leading to the formation of Cu clusters during the oxidation process. Therefore, the majority of Cu clusters, concentrated in the center of oxidized interface, could be also responsible for the enhanced ductility of the diffusion bonded MGs. In other words, during the welding process, those Cu clusters play an important role, as low-temperature solder, firmly bonding the MG blocks together while providing high ductility of the diffusion bonded MGs under plastic deformation. The oxidized interface is found to be stable, as shown in Fig. 7 (b). As the welding temperature is increased, the internal energy of MGs increases and becomes less stable. In contrast, the internal energy of the diffusion bonded

MGs decreases at higher welding temperature. Such a phenomenon is obviously related with the oxidized interface or GGI and indicates a much stable structure of oxidized interface. In addition, the absolute average GGI energy is positively correlated with the welding temperature, which implies an excellent stability of oxidized interface at high welding temperatures, as shown in Fig. 7 (c).

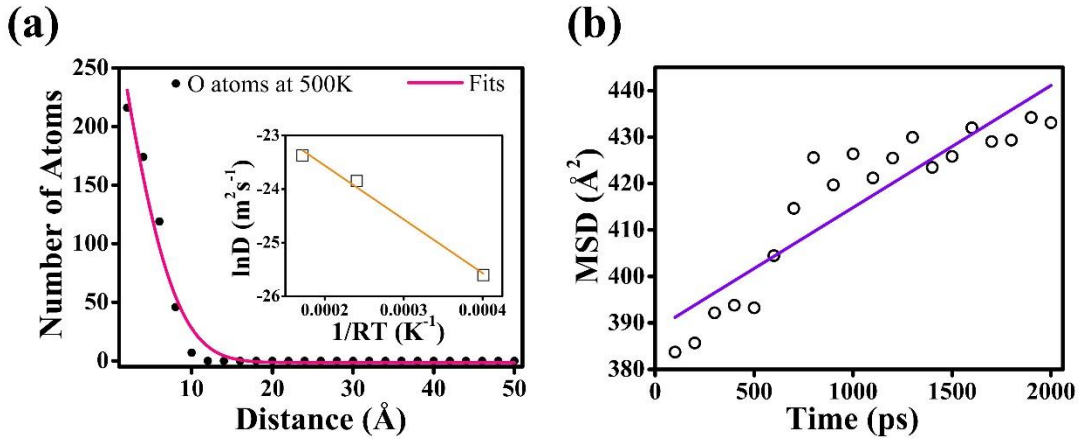

Fig. 8. Diffusion analysis on O atoms during the oxidization at the MG interface at 500 K by applying (a) Fick's second law of diffusion (at t=2 ns), and (b) Einstein relation. The inset in (a) is the fits of diffusion coefficient D by using Arrhenius equation.

In order to explain the heterogeneous atomic structure and position-dependent chemical composition around the GGIs, the analysis on diffusions of Zr, Cu and O atoms during oxidation processes is conducted. At the surface of MG under oxidization, Fick's second law or non-steady state diffusion could be used to analyze the diffusion coefficients of Zr, Cu and O atoms and the relation is expressed in the following equation

$$\frac{c_x - c_0}{c_s - c_0} = 1 - \mathrm{erf}\left(\frac{x}{2\sqrt{Dt}}\right) \quad , \tag{3}$$

where c_x is the concentration at position x, c_s is the surface concentration of diffusing atoms, c_0 is the uniform concentration of diffusing atoms away from the surface, D is the diffusion coefficient and t is time. For the diffusion coefficient of each atom type inside the MG block, Einstein relation is applied, and the corresponding equation could be expressed as

$$MSD = 6\ D\ t + C \quad , \tag{4}$$

where MSD is the mean square displacement for each atom type and C is the constant. Finally, the activation energy of diffusion for each element is determined by Arrhenius relation, as follows:

$$D = D_0 e^{\frac{E_a}{RT}} \quad , \tag{5}$$

where E_a is the activation energy, R is the universal gas constant, T is the temperature in Kelvin and D_0 is the maximal diffusion coefficient. Diffusion analysis at the interface under oxidization is performed in every 100 ps at different oxidization temperatures. Meanwhile, the diffusion coefficient inside the MG block is obtained when mean square displacement and its corresponding time follow a linear relationship. Taking the diffusions of O atoms as examples, Fig. 8(a) and (b) shows the determination on the diffusion coefficients D at the surface and in the interior of MG blocks during oxidation processes, using Eqs. (3) and (4), respectively. The

activation energy of diffusion of O atoms is determined by Eq. (5), as shown in the inset of Fig. 8(a).

Table I. The diffusion coefficients and activation energies of Zr, Cu and O atoms at the surface and in the interior of MG blocks during oxidization

Element Type		Diffusion Coefficient (m^2 s^{-1})			Activation Energy E_a (kJ mol^{-1})
		300 K	500 K	700 K	
Surface of MG block	Zr	5.71×10^{-13}	1.13×10^{-12}	2.20×10^{-12}	5.88
	Cu	7.29×10^{-12}	8.32×10^{-12}	7.56×10^{-11}	11.8
	O	5.32×10^{-12}	6.93×10^{-12}	2.44×10^{-11}	8.24
Interior of MG block	Zr	4.03×10^{-13}	2.02×10^{-12}	5.33×10^{-12}	11.1
	Cu	4.27×10^{-13}	2.73×10^{-12}	9.32×10^{-12}	13.3
	O	7.60×10^{-12}	4.38×10^{-11}	7.09×10^{-11}	10.0

As listed in Table I, the diffusion coefficient of Zr atoms at the surface under oxidization is much lower than those of Cu atoms and O atoms. Consequently, the Cu atoms could diffuse to and aggregate at the outer layer of the oxidized surface of the MG block, while O atoms could diffuse into the interiors of MG block and interact with Zr atoms to form the ZrO_2 clusters, as shown in Fig. 7(a). Thus, the fact that after the diffusion bonding processes there is broken concentration homogeneity of Cu and Zr atoms in the GGIs, as shown in Fig. 5, can be well explained. In the diffusion bonded MGs, Cu atoms in the center of GGI could have the highest concentration, as shown in Fig. 5(a) and Fig. 7(a), and could serve as low-temperature solders during the welding process. In contrast, Zr atoms tend to form stable ZrO_2 clusters away from the center of GGI because of the fast diffusion of O atoms from the oxidized surface into the interior of MG blocks.

IV. CONCLUSION

In summary, a novel low-temperature welding technique for MG is investigated by MD simulation. The diffusion bonding of Zr-Cu MGs with pre-oxidized surfaces is found to result in the enhanced mechanical properties of MGs when the bonding temperature and aspect ratio of the MG blocks are properly chosen. The GGIs in the diffusion bonded MGs are characterized by the presence of segregated Cu and ZrO_2 clusters, mainly resulting from the fast diffusions of Cu atom to the center of interface and the diffusion of oxygen atoms into the interior of MG blocks. The effects of GGIs on the plastic deformation of diffusion bonded MGs are investigated. This study paves a new avenue to overcome the longstanding issue of size limitation on MGs.

Acknowledgements

This work was supported by a grant from the Research Grants Council of the Hong Kong Special Administrative Region, China (PolyU152607/16E).

References

1 Y. Shen, X.C. Zheng, and G.P. Zheng, *Metall. Mater. Trans. A*, 2011, vol. 42, pp. 211–8.

2 T. Burgess and M. Ferry, *Mater. Today*, 2009, vol. 12, pp. 24–32.

3 Y. Kawamura, T. Shoji, and Y. Ohno, *J. Non. Cryst. Solids*, 2003, vol. 317, pp. 152–7.

4 J. Kim and Y. Kawamura, *Scr. Mater.*, 2007, vol. 56, pp. 709–12.

5 C.H. Wong and C.H. Shek, *Scr. Mater.*, 2003, vol. 49, pp. 393–7.

6 Y. Kawamura and Y. Ohno, *Scr. Mater.*, 2001, vol. 45, pp. 279–85.

7 Y. Kawamura and Y. Ohno, *Scr. Mater.*, 2001, vol. 45, pp. 127–32.

8 H. Gleiter, *Beilstein J. Nanotechnol.*, 2013, vol. 4, pp. 517–33.

9 H. Gleiter, T. Schimmel, and H. Hahn, *Nano Today*, 2014, 9, vol. 9.

10 P. Zhou, Q. Li, P. Gong, X. Wang, and M. Zhang, *Microelectron. Eng*, 2020, vol. 229, pp. 1113-63.

11 C. Guo, Y. Fang, B. Wu, S. Lan, G. Peng, X.L. Wang, H. Hahn, H. Gleiter, and T. Feng, *Mater. Res. Lett.*, 2017, vol. 5, pp. 293–9.

12 O. Adjaoud and K. Albe, *Acta Mater.*, 2018, vol. 145, pp. 322–30.

13 O. Adjaoud and K. Albe, *Acta Mater.*, 2016, vol. 113, pp. 284–92.

14 D. Şopu, Y. Ritter, H. Gleiter, and K. Albe, *Phys. Rev. B*, 2011, vol. 83, pp. 1–4.

15 B. Cheng and J.R. Trelewicz, *J. Mater. Res.*, 2019, vol. 34, pp. 2325–36.

16 O. Adjaoud and K. Albe, *Acta Mater.*, 2019, vol. 168, pp. 393–400.

17 D. Şopu and K. Albe, *Beilstein J. Nanotechnol.*, 2015, vol. 6, pp. 537–45.

18 Z.D. Sha, P.S. Branicio, Q.X. Pei, Z.S. Liu, H.P. Lee, T.E. Tay, and T.J. Wang, *Nanoscale*, 2015, vol. 7, pp. 17404–9.

19 K. Albe, Y. Ritter, and D. Şopu, *Mech. Mater.*, 2013, vol. 67, pp. 94–103.

20 S. Adibi, P.S. Branicio, Y.W. Zhang, and S.P. Joshi, *J. Appl. Phys*, 2014. vol. 116, pp. 043522-1.

21 Y. Ritter, D. Opu, H. Gleiter, and K. Albe, *Acta Mater.*, 2011, vol. 59, pp. 6588–93.

22 S. Adibi, P.S. Branicio, and S.P. Joshi, *Sci. Rep.*, 2015, vol. 5, pp. 1–9.

23 Y. Zhao, X. Peng, C. Huang, B. Yang, N. Hu, and M. Wang, 2019, vol. 9, pp. 1–17.

24 S.H. Nandam, O. Adjaoud, R. Schwaiger, Y. Ivanisenko, M.R. Chellali, D. Wang, K. Albe, and H. Hahn, *Acta Mater.*, 2020, vol. 193, pp. 252–60.

25 M. Zhang, Q.M. Li, J.C. Zhang, G.P. Zheng, and X.Y. Wang, *J. Alloys Compd.*, 2019, vol. 801, pp. 318–26.

26 S. Plimpton, *J. Comput. Phys.*, 1997, vol. 117, pp. 1–42.

27 P. Hirel, *Comput. Phys. Commun.*, 2015, vol. 197, pp. 212–9.

28 Y.Q. Cheng and E. Ma, *Prog. Mater. Sci.*, 2011, vol. 56, pp. 379–473.

29 T. Liang, T.R. Shan, Y.T. Cheng, B.D. Devine, M. Noordhoek, Y. Li, Z. Lu, S.R. Phillpot, and S.B. Sinnott, *Mater. Sci. Eng. R Reports*, 2013, vol. 74, pp. 255–79.

30 A. Stukowski, *Model. Simul. Mater. Sci. Eng.*, 2010, vol. 18, pp. 015012-7.

31 M.L. Falk and J.S. Langer, *Phys. Rev. E*, 1998, vol. 57, p. 14.

32 F. Shimizu, S. Ogata, and J. Li, *Mater. Trans.*, 2007, vol. 48, pp. 2923–7.

33 J. Li and F. Shimizu, *Report*, 2005, vol. 0, pp. 4–6.

34 Y.Q. Cheng, A.J. Cao, and E. Ma, *Acta Mater.*, 2009, vol. 57, pp. 3253–67.

35 C. Piconi, G. Maccauro, *Biomaterials*, 1999, vol. 20, pp. 1-25.